



CrossMark
click for updates

Cite this: *RSC Adv.*, 2014, 4, 37085

Metal ionic size directed complexation in manganese(II) coordination chemistry: efficient candidates showing phenoxazinone synthase mimicking activity†

Anangamohan Panja*

The present report describes the syntheses and structural characterizations of two new mononuclear manganese(II) complexes, $[\text{Mn}(\text{L}^1)\text{Cl}_2] \cdot 2\text{MeOH}$ (**1**) and $[\text{Mn}(\text{L}^2)\text{Cl}_2]$ (**2**), in which L^1 and L^2 are tetradentate ligands. Although the previous studies described that ligand L^1 exclusively binds the metal centers (Fe^{2+} , Ni^{2+} and Zn^{2+}) in the acyclic isomeric form (Schiff dibasic) of the ligand, in the present investigation it selectively binds Mn^{2+} ion in its cyclic (hexahydropyrimidine) analogue during the complexation reaction as evidenced by X-ray crystallography. The structure of **2** is quite interesting as it shows that one arm of the Schiff dibasic form of the ligand has been hydrolyzed, suggesting that these types of ligands with the Schiff dibasic form are incapable of yielding the stable manganese(II) complexes. The metal ionic size directed hydrolysis of one arm of the ligand has been confirmed by IR spectral studies. Both the complexes are reactive towards the oxidation of *o*-aminophenol (OAPH), and their relative catalytic efficiencies can be clearly explained by considering the steric contribution from the ligands and the electrochemical responses of the metal center. From the experimental data, a nice correlation, wherein the lower the $E_{1/2}$ value the higher the catalytic activity, can be drawn between $E_{1/2}$ and V_{max} of the complexes. The kinetics study exhibited a deuterium kinetic isotope effect in the catalytic oxidative coupling of two moles of OAPH by O_2 as evidenced by the 1.6 times rate retardation in the deuterated solvent, suggesting hydrogen atom transfer in the rate-determining step from the substrate hydroxy group to the metal-bound superoxo species.

Received 15th April 2014

Accepted 30th July 2014

DOI: 10.1039/c4ra03427a

www.rsc.org/advances

Introduction

Schiff-base complexes that contain a carbon–nitrogen double bond have been extensively studied in coordination chemistry, mainly due to their ease of synthesis, tremendous structural diversities, and enormous possibilities towards various applications, including catalysis.^{1–3} In addition, they can easily undergo reversible reactions under certain conditions, such as *E–Z* isomerization reactions, nucleophilic additions, transamination reactions, tautomerism, and aza Diels–Alder reactions. Among these, the condensation reactions of aromatic aldehydes with α,ω -di-primariopolyamines that contain both the primary and secondary amines are known to afford both Schiff dibases and their isomers with saturated heterocyclic rings (imidazolidine or hexahydropyrimidine).^{4,5} Isomerization among these products through formation or opening of the heterocyclic ring in the presence of metal ions is quite common

and two factors, namely, Lewis acidity and the size of the metal ions, are mainly responsible in such isomerization processes.^{6,7} Boča *et al.*^{8,9} have concluded that the relative acidity of imine-C and metal centers ultimately determine the direction in which the isomerization of the ligand will shift. For example, weak Lewis acids, such as Fe^{2+} , Co^{2+} , and Cu^{2+} , are incapable (or only partly capable) of opening the heterocyclic ring, whereas stronger Lewis acids (*e.g.*, Fe^{3+} and Zn^{2+}) can readily do it in order to gain the denticity of the ligands. In contrast, Tuchagues *et al.*¹⁰ postulated that, for each specific cation, the size of the metal ion is the determining factor in shifting the ligand equilibrium towards the most appropriate tautomeric form. For instance, low-spin Fe^{2+} has a small enough ionic radius (75 pm) to fit inside the void provided by the imine isomers, while the ionic radius of Ni^{2+} (83 pm) is probably too large to allow the coordination of the imine tautomer, and thus it stabilizes the cyclic analogue.

We are working on the transition-metal complexes with pyridine containing ligands in order to develop the functional mimics of various oxidase (oxygenase) metalloenzymes.^{11–15} These studies are helpful in getting an insight of the natural systems in which metalloenzymes facilitate the spin-forbidden

Postgraduate Department of Chemistry, Panskura Banamali College, Purba Medinipur, Panskura RS, West Bengal 721 152, India. E-mail: ampanja@yahoo.co.in

† Electronic supplementary information (ESI) available: Fig. S1–S5. CCDC 962739 and 997081. For ESI and crystallographic data in CIF or other electronic format see DOI: 10.1039/c4ra03427a

interaction between dioxygen and organic matter in the various biochemical reactions^{16–18} and ultimately provide a clue for the development of bioinspired catalysts for the oxidation reactions in the industrial and synthetic processes. Our recent reports revealed that cobalt complexes with pyridine-containing ligands are good functional models for the phenoxazinone synthase irrespective of the oxidation state of cobalt.¹⁴ This multicopper oxidase is found naturally in the bacterium *Streptomyces antibioticus*^{19,20} and catalyzes the oxidative coupling of two molecules of substituted *o*-aminophenol to the phenoxazinone chromophore in the final step for the biosynthesis of actinomycin D.²¹ The latter is used clinically for the treatment of Wilm's tumor, gestational choriocarcinoma, and other tumors in which phenoxazinone chromophore is recognized to inhibit DNA-dependent RNA synthesis by intercalation to DNA.^{22,23} In addition to copper-based models, some functional models of other metal ions, e.g. Fe³⁺, Mn²⁺ and Co^{2/3+}, have also been reported.^{11–15,24–31} Moreover, few structure–property correlations that were determined are sufficiently not wide but applicable only for a set of few compounds; therefore, phenoxazinone synthase activity of new systems should be explored to get better insight and more straightforward structure–property correlations.

Our recent reports disclosed that the cobalt ion exclusively shows selectivity towards the Schiff dibasic form of the ligands derived from the condensation of pyridine-2-aldehyde with α,ω -di-primariopolyamines, and even this selectivity is found to be insensitive to the oxidation states of cobalt, while manganese(II) ion prefers to bind with their cyclic analogue.^{14,15} The size of the manganese(II) ion is too large to fit inside the cavity provided by the Schiff dibasic form of the ligands thus preferring the cyclic analogue, which is consistent with the proposition made by Tuchagues *et al.*¹⁰ In order to check whether manganese(II) ion exclusively selects the cyclic isomer over its Schiff dibasic form, in the present investigation, the coordination ability of manganese(II) ion has been tested with the ligands derived from the condensation of a triamine with longer propylenic linkers and pyridine-2-aldehyde (or 2-acetylpyridine). Syntheses and structural characterizations of two new manganese(II) complexes, [Mn(L¹)Cl₂]·2MeOH (1) and [Mn(L²)Cl₂] (2), have been reported in which L¹ and L² are tetradentate ligands, as depicted in Scheme 1. The phenoxazinone synthase-like activity and its detailed kinetic studies to evaluate various kinetic parameters, including the turnover number for both the complexes, have also been described.

Experimental section

Materials and physical measurements

Chemicals such as pyridine-2-aldehyde, 2-acetylpyridine and 3,3'-iminobis(propylamine) (Aldrich), and manganese(II) chloride tetrahydrate and *o*-aminophenol (Merck, India) of reagent grade were used without further purification. Solvents like methanol, CD₃OD and diethyl ether (Merck, India) of analytical grade were used as received.

Elemental analysis for C, H and N were carried out using a PerkinElmer 240 elemental analyzer. The infrared spectra of the

complexes in KBr pellets were recorded in the range of 400–4000 cm⁻¹ on a PerkinElmer Infrared spectrum two spectrometer. Electronic absorption spectra were recorded using a PerkinElmer Lambda-35 spectrophotometer with a 1 cm-path-length quartz cell. Cyclic voltammetry measurements were performed on an EG&G Princeton Applied Research potentiostat model 263A with a conventional three electrode system using a Pt working electrode, Pt auxiliary electrode and Ag/AgCl reference electrode. Electrospray ionization mass (ESI-MS positive) spectra were recorded on a micromass Q-TOF mass spectrometer.

Synthesis of [Mn(L¹)Cl₂]·2MeOH (1)

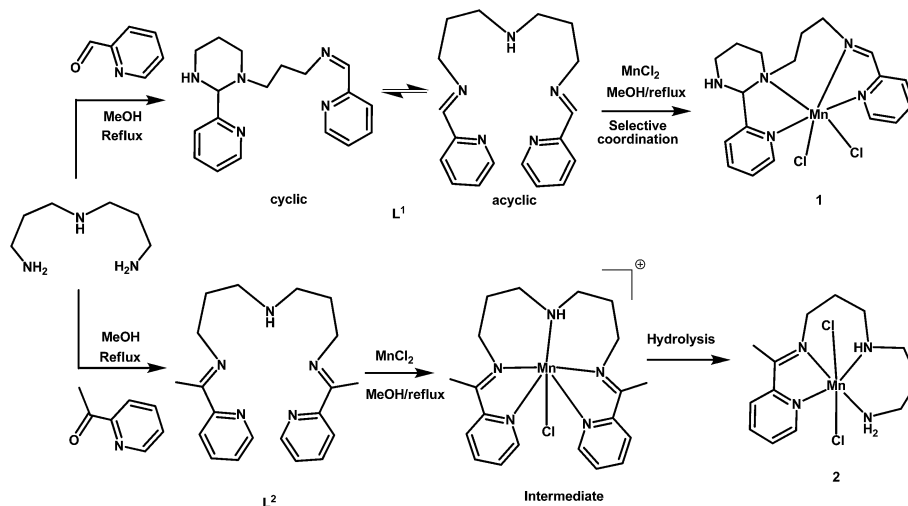
A mixture of pyridine-2-aldehyde (0.428 g, 4.0 mmol) and 3,3'-iminobis(propylamine) (0.262 g, 2.0 mmol) in 30 ml of methanol was refluxed for 30 min. To the resulting yellow solution a methanol solution of MnCl₂·4H₂O (0.396 g, 2 mmol) was added, and the mixture was further allowed to reflux for 30 min. The solution was allowed to cool to room temperature, and on addition of ether, a pale-yellow powder separated out from the solution. The precipitate was collected by filtration, washed with methanol/ether solution, and air dried, and a yield of 0.800 g (83%) was obtained. Crops of pale-yellow crystals suitable for X-ray analysis were obtained from the slow diffusion of ether into a methanolic solution of the complex. Anal. calcd for C₁₉H₂₇Cl₂MnN₅O₂ expected: C, 48.11%; H, 6.25%; N, 14.02%. Found: C, 47.67%; H, 6.00%; N, 14.08%. IR (KBr, cm⁻¹): 3348 br ($\nu_{\text{N-H}}$ and $\nu_{\text{O-H}}$); 1646 s ($\nu_{\text{C=N}}$, imine); 1597 s ($\nu_{\text{C=N}}$, pyridine). A major peak was detected at $m/z = 399.07$ corresponding to [Mn(L¹)Cl]⁺.

Synthesis of [Mn(L²)Cl₂] (2)

A similar synthetic methodology was applied using 2-acetylpyridine (0.488 g, 4.0 mmol), 3,3'-iminobis(propylamine) (0.262 g, 2.0 mmol) and MnCl₂·4H₂O (0.396 g, 2 mmol) as starting materials, and 0.574 g (80%) of a pale-yellow precipitate was obtained. Crops of dark-yellow crystals suitable for X-ray analysis were obtained from slow diffusion of ether into a methanol solution of complex 2. Anal. calcd C₁₃H₂₂Cl₂MnN₄: C, 43.35%; H, 6.15%; N, 15.55%. Found: C, 43.37%; H, 6.27%; N, 15.38%. IR (KBr, cm⁻¹): 3239 br ($\nu_{\text{N-H}}$); 1645 s ($\nu_{\text{C=N}}$, imine); 1598 s ($\nu_{\text{C=N}}$, pyridine). A base peak was detected at $m/z = 324.09$ corresponding to [Mn(L²)Cl]⁺.

X-ray crystallography

Single crystal X-ray diffraction data for complexes 1 and 2 were obtained on a Bruker SMART APEX-II CCD diffractometer using graphite monochromated Mo-K α radiation. The unit cell was determined from the setting angles of 36 frames of data. Several scans in ϕ and ω directions were made to increase the number of redundant reflections and were averaged during the refinement cycles. Data processing for both the complexes were performed using the Bruker Apex2 suite.³² Reflections were then corrected for absorption, inter-frame scaling, and other systematic errors with SADABS.³² All the structures were solved by direct methods, and all non-hydrogen atoms were refined by the full-matrix least squares based on F^2 using the SHELXL-97³³ program using the



Scheme 1 Synthetic route to complexes 1 and 2.

WINGX package.³⁴ Hydrogen atoms attached to carbon atoms were included in the structure factor calculation in geometrically idealized positions, while those connected to nitrogen and oxygen atoms were located in the difference Fourier maps. Using a riding model, the hydrogen atoms were isotropically treated with their isotropic displacement parameters depending on the parent atoms. Relevant crystallographic data along with refinement details for the complexes are given in Table 1.

Kinetics of the phenoxazinone synthase activity

In a typical experiment, complexes 1 or 2 were mixed with *o*-aminophenol (OAPH) in air-saturated methanol and the

oxidation of OAPH was investigated spectrophotometrically by monitoring the growth of the absorbance as a function of time at 435 nm ($\epsilon = 24 \times 10^3 \text{ M}^{-1} \text{ cm}^{-1}$),²⁷ which is a characteristic absorbance of 2-aminophenoxazin-3-one in methanol. To determine the dependence of the rate of the reaction on substrate concentration and to evaluate various kinetic parameters, $1 \times 10^{-4} \text{ M}$ solutions of the complexes were treated with at least 10 equivalents of substrate in order to maintain the pseudo-first order condition. Similarly, varying amounts of catalyst ($5\text{--}100 \times 10^{-5} \text{ M}$) were mixed with a fixed concentration ($1 \times 10^{-2} \text{ M}$) of substrate in methanol (2.0 ml) saturated with dioxygen in order to examine the dependence of the rate of the

Table 1 Crystal data and structure refinement for complexes 1 and 2

	1	2
Empirical formula	$\text{C}_{20}\text{H}_{31}\text{Cl}_2\text{MnN}_5\text{O}_2$	$\text{C}_{13}\text{H}_{22}\text{Cl}_2\text{MnN}_4$
Formula weight	499.34	360.19
Temperature (K)	293(2)	150(2)
Wavelength (Å)	0.71073	0.71073
Crystal system	Monoclinic	Monoclinic
Space group	$P2_1/c$	$C2/c$
<i>a</i> (Å)	10.4242(2)	19.2620(3)
<i>b</i> (Å)	9.1757(1)	11.7960(1)
<i>c</i> (Å)	24.4086(5)	17.1290(3)
β (°)	100.971(1)	122.207(5)
Volume (Å ³)	2292.00(7)	3293.09(20)
<i>Z</i>	4	8
$D_{\text{calc.}}$ (g cm ⁻³)	1.401	1.453
μ (mm ⁻¹)	0.833	1.122
<i>F</i> (000)	1004	1496
θ range (°)	2.80–30.08	2.90–32.05
Limiting indices	$-14 \leq h \leq 14, -12 \leq k \leq 12, -33 \leq l \leq 34$	$-28 \leq h \leq 28, -17 \leq k \leq 17, -25 \leq l \leq 25$
Reflections collected	23 831	10 331
Independent reflection/ <i>R</i> _{int}	6697/0.0592	5725/0.0159
Observed reflections	4739	5238
Data/restraints/parameters	6697/0/310	5725/0/185
Goodness-of-fit on <i>F</i> ²	1.043	1.071
Final <i>R</i> indices [<i>I</i> > 2σ(<i>I</i>)]	<i>R</i> 1 = 0.0482, w <i>R</i> 2 = 0.1286	<i>R</i> 1 = 0.0279, w <i>R</i> 2 = 0.0645
<i>R</i> indices (all data)	<i>R</i> 1 = 0.0791, w <i>R</i> 2 = 0.1441	<i>R</i> 1 = 0.0279, w <i>R</i> 2 = 0.0710
Largest diff. peak/hole (e Å ⁻³)	0.881/−0.766	0.514/−0.528

reaction on catalyst concentration. The initial rate method was applied to determine the rate of a reaction, and the average initial rate over three independent measurements was determined by linear regression from the slope of absorbance *versus* time plot.

Results and discussion

Syntheses and general characterizations

The condensation of a polyamine with pyridine-2-aldehyde in 1 : 2 molar ratio yields a mixture of Schiff dibase and its heterocyclic analogue, and the ratio of which can be examined by the NMR spectroscopy.^{9,10,35} Recent reports revealed that the metal-assisted ring opening/closing processes are common for such ligand systems, and several factors are responsible in this isomerization process, including the size of the metal ions, Lewis acidity, and the stereochemistry of the metal centers.^{9,10,35} We have recently examined the coordination ability of manganese(II) ion with this class of ligands derived from the condensation of two different triamines with pyridine-2-aldehyde, and the results show the selective complexation ability of manganese(II) ion with the cyclic form of the ligands.¹⁵ In order to explore whether the manganese(II) ion exclusively selects the cyclic isomeric form, in the present work, the ligands derived from the condensation of two equivalents of pyridine-2-aldehyde (or 2-acetylpyridine) and one equivalent of 3,3'-imino-bis(propylamine) with two longer propylenic linkers were allowed to react with the hydrated salt of manganese(II) chloride in methanol (Scheme 1). On the basis of the characterizations of the complexes, including X-ray crystal structures (*vide infra*), they are formulated as $[\text{Mn}(\text{L}^1)\text{Cl}_2] \cdot 2\text{MeOH}$ (**1**) and $[\text{Mn}(\text{L}^2)\text{Cl}_2]$ (**2**). Complex **1** is as usual found in our recent report,¹⁵ but complex **2** is quite different as one arm of the Schiff base has been hydrolyzed during course of the reaction (*vide infra*).

In the IR spectra of complex **2**, a medium intense peak at 3239 cm^{-1} indicates N–H stretching vibration of the ligand; however, the N–H stretching band overlaps with the O–H stretching vibration of the lattice methanol molecules in **1**, and the resultant broad band was observed at 3348 cm^{-1} . In the IR spectra of both the complexes, a strong and sharp band due to azomethine $\nu(\text{C}=\text{N})$ appeared at 1646 and 1645 cm^{-1} , respectively. In addition, sharp peaks were observed at 1597 and 1598 cm^{-1} for complexes **1** and **2**, respectively, which might be assigned to the stretching vibration of pyridyl C=N bond.

Structural studies

The crystal structure of complex **1** along with the atom numbering scheme is depicted in Fig. 1, and selected bond lengths and angles are given in Table 2. Complex **1** crystallizes in the monoclinic $P2_1/c$ space group with two lattice methanol molecules, one of which is disordered over a crystallographic inversion center. Although ligand L^1 possesses one chiral center but the centrosymmetric space group suggests that the compound crystallizes as a racemate. The geometry of the metal center is a pseudo-octahedron comprised of two pyridyl, one amine (hexahydropyrimidine) and one imine nitrogen donors

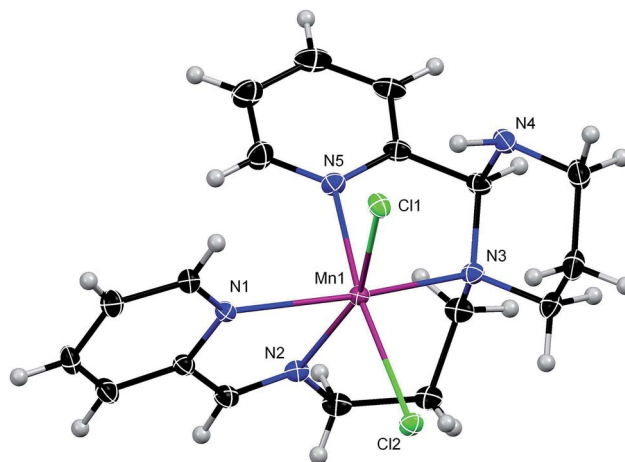


Fig. 1 Crystal structure of $\text{Mn}(\text{L}^1)\text{Cl}_2 \cdot 2\text{MeOH}$ (**1**) with the atom labeling scheme. Ellipsoids are drawn at the 50% probability level and solvent molecules are omitted for clarity.

from the folded dissymmetric ligand L^1 , and two exogenous chloride ions. In the crystal structure, both the folded dissymmetric pyridyl nitrogen atoms and two chloride ions are *cis* coordinated, and two pyridyl rings are approximately perpendicular to each other (dihedral angle: 86.30°). The Mn– N_{py} [$2.302(2)$ and 2.324 \AA] and Mn– N_{imine} [$2.302(2)\text{ \AA}$] distances are very similar but somewhat shorter than the Mn– N_{amine} [$2.367(2)\text{ \AA}$] distance, which is along the line of the state of hybridizations of

Table 2 Selected bond lengths (Å) and bond angles ($^\circ$) for **1** and **2**

1			
Mn1–N1	2.302(2)	Mn1–N5	2.324(2)
Mn1–N2	2.302(2)	Mn1–Cl1	2.4674(7)
Mn1–N3	2.367(2)	Mn1–Cl2	2.4620(7)
N1–Mn1–N2	71.69(7)	Cl1–Mn1–N1	89.80(5)
N1–Mn1–N3	158.37(8)	Cl1–Mn1–N2	160.94(6)
N1–Mn1–N5	93.63(8)	Cl1–Mn1–N3	105.41(6)
N2–Mn1–N3	91.35(8)	Cl1–Mn1–N5	90.46(6)
N2–Mn1–N5	86.30(8)	Cl2–Mn1–N1	98.19(5)
N3–Mn1–N5	71.38(8)	Cl2–Mn1–N2	86.74(6)
		Cl2–Mn1–N3	94.02(6)
		Cl2–Mn1–N5	163.64(6)
		Cl1–Mn1–Cl2	100.79(3)
2			
Mn1–N1	2.2536(9)	Mn1–N4	2.2284(9)
Mn1–N2	2.2434(9)	Mn1–Cl1	2.5781(3)
Mn1–N3	2.2266(9)	Mn1–Cl2	2.5535(3)
N1–Mn1–N2	72.60(3)	Cl1–Mn1–N1	88.07(2)
N1–Mn1–N3	166.36(3)	Cl1–Mn1–N2	97.45(3)
N1–Mn1–N4	100.61(3)	Cl1–Mn1–N3	88.37(3)
N2–Mn1–N3	94.83(3)	Cl1–Mn1–N4	84.40(3)
N2–Mn1–N4	172.83(4)	Cl2–Mn1–N1	93.91(2)
N3–Mn1–N4	92.13(4)	Cl2–Mn1–N2	84.47(2)
		Cl2–Mn1–N3	90.02(3)
		Cl2–Mn1–N4	93.87(3)
		Cl1–Mn1–Cl2	177.58(1)

nitrogen atoms. The Mn–Cl bond lengths are found to be 2.461(1) and 2.467(1) Å, and all the bond lengths are comparable to the related complexes with a similar environment.^{35–39} The degree of distortion from the ideal octahedral geometry (90°/180°) is reflected from both the cisoid and transoid angles as shown in Table 2. Such distortion from the ideal octahedral geometry is presumably due to the shorter bite angles of the dissymmetric ligands, especially for those forming five-membered chelate rings. Five-membered chelates involving imine-N are conjugated and as expected have a nearly planar conformation, while the remaining one is in the envelope conformation indicating a saturated non-planar characteristic. Moreover, the six-membered hexahydropyrimidine rings are in a more stable chair conformation as found in the most of the systems.¹⁰ The secondary amine hydrogen atom of hexahydropyrimidine ring undergoes an intramolecular hydrogen bonding with a coordinated Cl atom, the dimension of which is given in Table 3. In addition, the secondary amine nitrogen atom forms a hydrogen bond with the ordered solvent methanol molecule in **1**. The disordered molecule of methanol solvent, sitting on an inversion center, also forms hydrogen bonds with two adjacent ordered molecules of methanol (Table 3). These hydrogen bonds along with the edge-to-edge π - π stacking interaction (3.422 Å) lead to the formation of a 3D supramolecular network of **1**, as shown in Fig. S1.†

The crystal structure of compound **2** is presented in Fig. 2, and principle bond lengths and angles are listed in Table 2.

Table 3 Geometry of important hydrogen bonds (Å, °) for **1** and **2**^a

	D–H...A	D–H	H...A	D...A	<D–H...A
1	O2–H1A...N4	0.82	2.03	2.836(5)	168
	O2–H2A...O1	0.93	1.98	2.842(13)	152
	N4–H4...Cl1	1.00	2.36	3.285(4)	154
2	N3–H3A...Cl1a	0.89	2.58	3.318(1)	140
	N4–H4B...Cl2b	0.90	2.47	3.357(1)	167

^a Symmetry code: $a = 1/2 - x, -1/2 - y$ and $-z$; $b = 1/2 - x, 1/2 - y$ and $-z$.

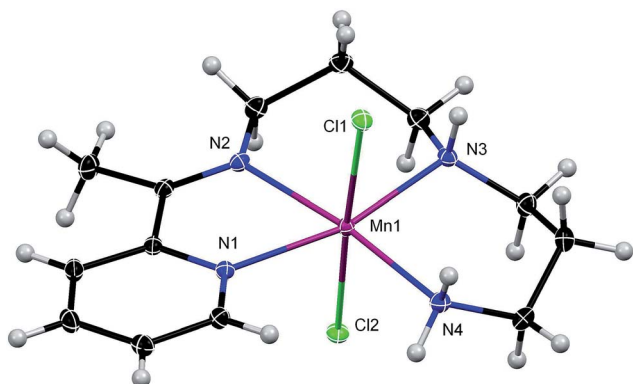


Fig. 2 Molecular structure of Mn(L²)Cl₂ (**2**) with the atom labeling scheme. Ellipsoids are presented at the 50% probability level.

Complex **2** crystallizes in the monoclinic $C2/c$ space group in which the complex molecule sits in a general position. The manganese(II) ion is in a distorted-octahedral environment, comprised of the four nitrogen atoms of the L² ligand in the equatorial plane and two exogenous chloride anions in the apical positions. The Mn–Cl and Mn–N distances are similar to what is observed for the manganese(II) complexes of similar coordination environments. Several bond angles in **2** (Table 2) deviate significantly from the ideal value of 90° or 180°, a characteristic of a regular octahedron. The crystal packing of complex **2** is mainly stabilized by moderately strong hydrogen bonding interactions between amine-H and coordinated Cl[−] ions (Table 3), which leads to the construction of a supramolecular 1D chain propagating along the b axis (Fig. 3). These supramolecular chains further interact with each other by means of C–H... π stacking interaction (2.951 Å), which forms a 2D sheet in the ab plane.

Metal-catalyzed hydrolysis of imine bond

The crystal structure of complex **1** shows that the manganese(II) ion again selects the cyclic isomer for stability during the complexation process.¹⁵ Tuchagues *et al.*¹⁰ reported a number of complexes having different metal ions (Fe²⁺, Ni²⁺ and Zn²⁺) with three different ligand systems. They found that regardless of the metal ions, the cyclic form of the ligand derived from a triamine with two shorter ethylenic linkers is stabilized through tetra-coordination, while the acyclic Schiff dibasic isomer of L¹ (derived from a triamine with two longer propylenic linkers) is stabilized through penta-coordination in order to gain extra stability by increasing the donor sites. Based on the observations, they concluded that size of the metal ions is a determining factor over Lewis acidity for the stability of the different isomeric forms of the ligands in the complexation process. Unlike their observation, the longer propylenic linkers of the

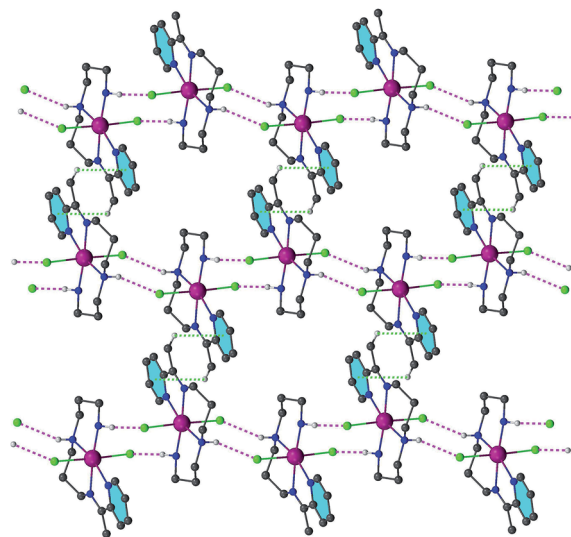


Fig. 3 Molecular packing showing hydrogen bonding and C–H... π interactions in complex **2**; hydrogen atoms not participating in hydrogen bonding are omitted for clarity.

present triamine (in L^1) are unable to stabilize the Schiff dibasic form of the ligand in the manganese(II) coordination compound. The ionic radius of Mn^{2+} is even larger than Fe^{2+} , Ni^{2+} and Zn^{2+} ; thus, the Schiff dibasic form of ligand L^1 is unable to accommodate the Mn^{2+} ion. This result further strengthens the proposition made by Tuchagues and coworkers that the size of the metal ions plays a critical role in selective coordination of the ligands in the complexes with either cyclic or acyclic isomer. In order to further confirm whether the manganese(II) ion has any tendency to stabilize the Schiff dibasic form, a similar experiment was carried out with the ligand derived from the condensation of the same triamine with 2-acetylpyridine, which is expected to produce only the Schiff dibasic ligand because methyl substitution on the azomethine-C not only reduces the electrophilic character of the imine-C but also increases the steric hindrance to the approaching nucleophile. However, the structural study of complex **2** indicates that one arm of the Schiff base has been hydrolyzed. In our recent report, we have shown that the *in situ* condensation of 3,3'-iminobis(propylamine) and 2-acetylpyridine, followed by the addition of cobalt(II) salt, yielded a dinuclear cobalt(III) complex in which the Schiff dibasic ligand was coordinated to the metal centers.¹⁴ IR spectral studies of solution were carried out to check whether the complex **2** arises from the hydrolysis of one arm of the Schiff dibasic ligand instead of the half condensation reaction of triamine and 2-acetylpyridine (1 : 1 condensation). The *in situ* prepared ligand derived from the condensation of 3,3'-iminobis(propylamine) and 2-acetylpyridine in 1 : 2 molar ratio did not show any stretching of the keto group (Fig. 4). The absence of the stretching band for the keto group and the appearance of the stretching band of the azomethine group (at 1645 cm^{-1}) confirm the double condensation. Interestingly, on addition of manganese(II) chloride, a new band appeared at 1697 cm^{-1} , which is due to the free 2-acetylpyridine, and this

observation supports the hydrolysis of one arm of the ligand during the complexation process. The present results significantly conclude that the size of the manganese(II) ion is too large to allow the coordination of the Schiff dibasic form of the ligands, especially those derived from triamines and pyridine-2-aldehyde (or 2-acetylpyridine).

Cyclic voltammetry

The transition metal-based enzymes catalyze the redox processes in the biochemical reactions in which the redox potential of the metal centers plays an important role. Therefore, the electrochemical behaviors of their models are of profound importance as they could give us clues for their catalytic ability. The electrochemical behavior of the complexes was investigated in acetonitrile solution containing 0.1 M tetraethylammonium perchlorate (TEAP) as a supporting electrolyte. Cyclic voltammograms of complexes **1** and **2** are depicted in Fig. 5 and S2,[†] respectively, and the electrochemical data for both the complexes are summarized in Table 4. Scanning in the anodic direction revealed a reduction wave at 0.93 and 0.76 V for **1** and **2**, respectively, which is due to the oxidation of manganese(II) to manganese(III). On reversal of the scan direction, the resultant manganese(III) complex was reduced to manganese(II) at 0.75 and 0.61 V for **1** and **2**, respectively. These nearly quasi-reversible electrode responses for the $Mn(II)/Mn(III)$ oxidation process are in line with the closely related manganese(II) complexes of similar ligand environment.^{15,39,40} The $E_{1/2}$ value of 0.84 V for complex **1** is significantly higher than **2** (0.68 V), which might be due to the different electronic environments in these complexes. The higher σ donor ability of both the primary and secondary amine groups in L^2 pushes

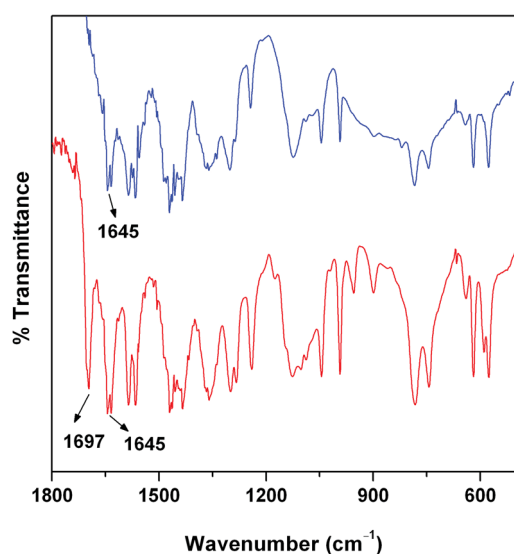


Fig. 4 IR spectra of the *in situ* prepared condensation of 3,3'-iminobis(propylamine) and 2-acetylpyridine in 1 : 2 molar ratio (top) and on addition of manganese(II) chloride (bottom).

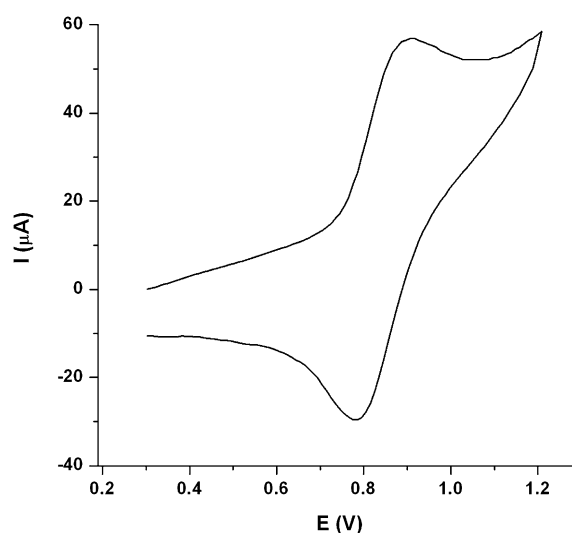


Fig. 5 Cyclic voltammogram of a 5 mM acetonitrile solution of **1** with a conventional three electrode system using a Pt working electrode, Pt auxiliary electrode and Ag/AgCl reference electrode in the presence of tetraethylammonium perchlorate (TEAP) as the supporting electrolyte at ambient temperature; scan rate: 100 mV s^{-1} .

Table 4 Electrochemical data for 1 and 2 in acetonitrile^a

Complex	E_p^c (V)	E_p^a (V)	ΔE_p (V)	$E_{1/2}$ (V)
1	0.75	0.93	0.18	0.84
2	0.61	0.76	0.15	0.68

^a Pt working and Ag/AgCl reference electrodes; supporting electrolyte is tetraethylammonium perchlorate; scan rate 100 mV s⁻¹; E_p^a and E_p^c are anodic and cathodic peak potentials, respectively; $E_{1/2} = 0.5(E_p^a - E_p^c)$; $\Delta E_p = E_p^a - E_p^c$.

more electron density towards the metal center, favoring the oxidation of the manganese(II) center in 2.

Phenoxazinone synthase-like activity

The reaction between *o*-aminophenol and dioxygen in the presence of a catalytic amount of complexes 1 or 2 was performed in dioxygen-saturated methanol because of the good solubility of the complexes, the substrate, and the final product in this solvent. In order to avoid the autoxidation of the substrate by air, the catalytic activity was examined in the absence of an added base. Before going to the detailed kinetic investigation, it is necessary to check the ability of the complexes to behave as catalysts for the oxidation of *o*-aminophenol. For this purpose, 1.0×10^{-4} M solutions of the complexes (1 or 2) were treated with a 0.01 M solution of OAPH, and the growth of the absorption band of the phenoxazinone chromophore at 435 nm as a function of time was observed, which indicates the catalytic oxidation of *o*-aminophenol to the corresponding 2-aminophenoxazin-3-one. A representative time-resolved spectral profile for a period of 2 h after the addition of OAPH for complex 1 is shown in Fig. 6. In order to establish the importance of the metal-complex conclusively in

the catalytic process, a control experiment was performed in which OAPH was treated only with ligand L¹, and the time-course data of the resulted solution was recorded at 435 nm, which did not show any significant growth of absorbance (Fig. S3†). On addition of the methanolic solution of complex 1 to the same solution, progressive increase in the peak intensity was noticed. These observations clearly conclude that the phenoxazinone synthase activity arises solely from the manganese(II) complexes.

In order to understand the degree of catalytic efficiency, kinetic studies of both the complexes were performed at 25 °C. For this purpose, 1×10^{-4} M solutions of the complexes were treated with at least a 10-fold concentrated substrate solution as that of the complex to maintain the pseudo-first-order condition. For a particular complex–substrate mixture, time scan at the maximum band for 2-aminophenoxazine-3-one was carried out for a period of 30 min, and the initial rate was determined by linear regression from the slope of the absorbance *versus* time plot. The initial rate of the reactions *versus* the concentration of the substrate plot shows rate saturation kinetics (Fig. 7). This observation indicates that formation of 2-aminophenoxazine-3-one proceeds through a relatively stable intermediate, a complex–substrate adduct, followed by the redox decomposition of the intermediate at the rate determining step. The initial rates *versus* the concentration of substrate data were then analyzed on the basis of the Michaelis–Menten approach of enzymatic kinetics to obtain the Lineweaver–Burk (double reciprocal) plot as well as values of the parameters V_{max} , K_M , and K_{cat} . The observed and simulated initial rates *versus* the substrate concentration plots for 1 and 2 are depicted in Fig. 7, while the Lineweaver–Burk plots are displayed in Fig. 8. Analyses of the experimental data yielded the Michaelis binding constant (K_M) value of $(1.11 \pm 0.08) \times 10^{-2}$ M for 1 and $(8.53 \pm 1.05) \times 10^{-3}$ M for 2, and the V_{max} values of $(6.54 \pm 0.42) \times 10^{-7}$ M⁻¹

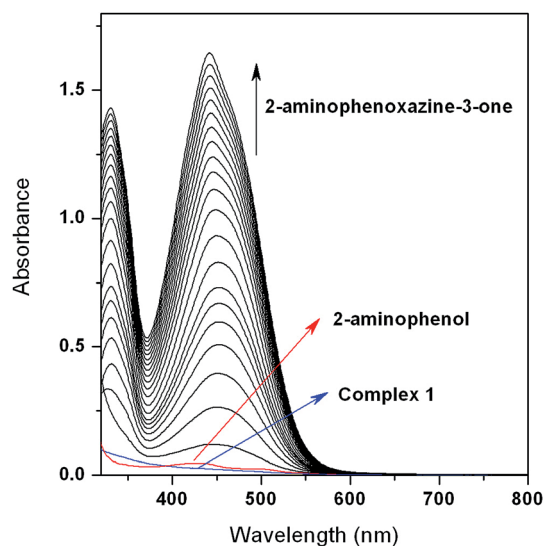


Fig. 6 UV-vis spectral profile showing the growth of phenoxazinone chromophore at 435 nm after the addition of *o*-aminophenol (0.01 M) to a solution of 1 (1×10^{-4} M) in methanol at 25 °C. The spectra were recorded for a period of 2 h.

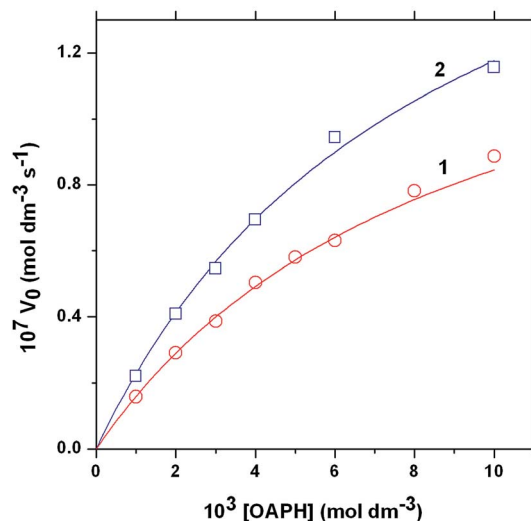


Fig. 7 Initial rate versus substrate concentration plot for the oxidation of *o*-aminophenol catalyzed by 1 and 2 in methanol. Symbols and solid lines represent the experimental and simulated profiles, respectively.

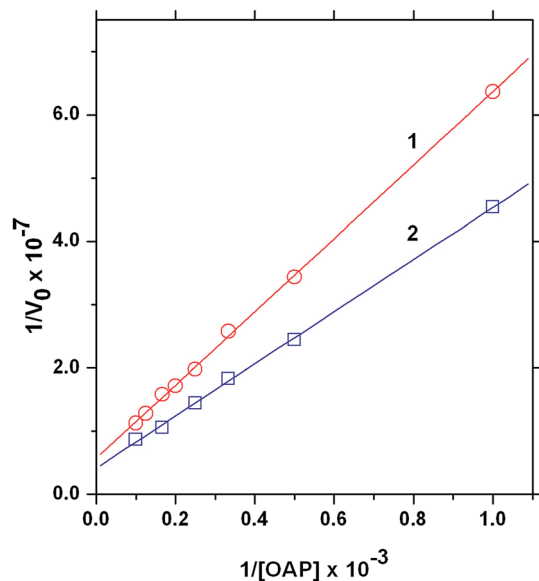


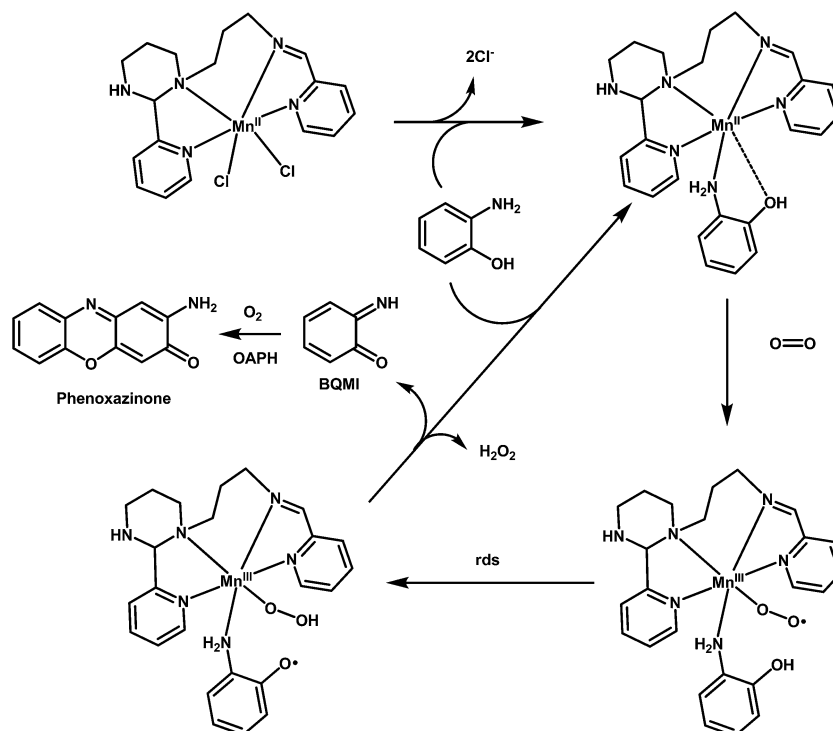
Fig. 8 Lineweaver–Burk plots for the oxidation of *o*-aminophenol catalyzed by **1** and **2** in methanol. Symbols and solid lines represent the experimental and simulated profiles, respectively.

and $(7.59 \pm 0.64) \times 10^{-7}$ for **1** and **2**, respectively. The turnover number (k_{cat}) value is obtained by dividing the V_{max} by the concentration of the complex used and is found to be 23.54 and 27.32 h^{-1} for **1** and **2**, respectively. Moreover, for a particular substrate concentration, when complex concentration was varied, a linear relationship for the initial rates was obtained, which shows a first-

order dependence of reaction on the complex concentration (Fig. S4†).

Comparative phenoxazinone synthase activity and probable mechanism

The reaction kinetics shows that both the complexes are very reactive towards the oxidation of *o*-aminophenol, and the rate saturation kinetics study clearly indicates that the reaction proceeds through the stable complex–substrate intermediate formation. In order to justify the involvement of molecular dioxygen in the catalytic cycle, the UV-vis spectra of a mixture of 1×10^{-4} M solution of complex **2** with 100 fold excess of OAPH were recorded in a nitrogen atmosphere, and no spectral growth at 435 nm was observed until one hour of mixing. This observation unambiguously proves that molecular dioxygen oxidizes OAPH to the corresponding 2-aminophenoxazine-3-one in the catalytic cycle in the presence of manganese(II) complex as a catalyst. Based on the above results, a plausible mechanism is attempted, involving stepwise pathways, keeping in mind that it is impossible to prove any single mechanism. A tentative catalytic cycle for the formation of the phenoxazinone chromophore is shown in Scheme 2. At the first step, OAPH forms an adduct with the manganese(II) complex,^{12,13} which yields an OAP radical by the reaction with molecular dioxygen in the rate determining step. The OAP radical may generate *o*-benzoquinone monamine (BQMI) in many ways, including oxidation by the manganese(III) center. Finally, 2-aminophenoxazine-3-one is produced *via* several oxidative dehydrogenation processes, involving OAPH, O_2 , and BQMI, as shown in Scheme 2. In order



Scheme 2 Plausible mechanistic pathway showing the formation of 2-aminophenoxazine-3-one in which complex **1** is chosen as model complex.

to increase the acceptability of the most probable mechanism, the mass spectral investigation of 1 : 50 mixture of complex **1** and OAPH were recorded after 10 minutes of mixing in methanol (Fig. S5†). The spectrum comprised of all the peaks that were only found for the complex, and these peaks at $m/z = 310.16$, 363.09 and 399.07 are due to the mono-cationic species of $(L^1 + H)^+$, $[Mn^{II}(L^1) - H]^+$ and $[Mn^{II}(L^1)Cl]^+$ as indicated by the isotopic distribution pattern together with the line-to-line separation of 1.0. In addition, one minor peak at $m/z = 472.15$ is quite interesting because the peak position and the line-to-line separation of unity clearly indicates that this peak arises due to 1 : 1 complex–substrate aggregate $[Mn^{II}(L^1)(OAP)]^+$, which is consistent with the earlier discussed rate saturation kinetics. However, the mass spectrum does not suggest any species related to the dioxygen bound metal-complex. In our recent report, we have observed that the acyclic dibasic form of ligand L^1 yielded a peroxo-bridged dinuclear cobalt(III) complex and that compound exhibited phenoxazinone synthase activity.¹⁴ Therefore, I speculated that in the present case, dioxygen-bound metal center could play an important role in the catalytic process. To determine whether manganese(III)-superoxo is the active species in abstracting the O–H proton of OAPH in the rate determining step, comparative kinetic studies were performed under a given set of conditions in both methanol and deuterated methanol. It can be assumed that in CH_3OD the phenolic-OH of OAPH undergoes a nearly complete exchange for OD. Consequently, if the rate-determining step involves the breaking of the –O–H (–O–D) bond, a kinetic isotope effect (KIE) should be observed upon changing the solvent from CH_3OH to CH_3OD . In fact, 1.6 times rate retardation in the deuterated solvent suggests that the hydrogen atom transfer in the rate-determining step from the substrate hydroxy group to the metal-bound superoxo species is operative in the catalytic oxidative coupling of two moles of OAPH by O_2 .²⁸ However, the turnover numbers suggest that complex **2** is more reactive than **1** towards the phenoxazinone synthase activity. It has been well explored that the catalytic activity of a complex depends on several factors such as the geometry of the complex, the redox potential of the central metal ion, and the steric factor. The present results can nicely be interpreted by considering the electrochemical potential along with the coordination environments around the metal center. Ligand L^2 in **2** is less bulky than L^1 in **1** and thus favors interaction of the substrate to the metal center. In addition, the lower electrochemical response of complex **2** facilitates the interaction of the metal center with molecular dioxygen in the catalytic cycle.

Conclusions

Two novel mononuclear manganese(II) complexes have been synthesized and structurally characterized by X-ray diffraction studies. Structural characterization reveals that the Mn^{2+} ion prefers the cyclic (hexahydropyrimidine) form of the ligand in **1**; however, in **2**, one arm has been hydrolyzed during the complexation reaction. It has already been reported that ligand L^1 exclusively binds the metal centers (Fe^{2+} , Ni^{2+} and Zn^{2+}) in the acyclic isomeric form of the ligand, but the higher ionic

radius of the Mn^{2+} ion enforces the stabilization of the cyclic analogue during complexation. IR spectral results demonstrate that the size of manganese(II) ion is too large to allow the coordination of the Schiff dibasic form of the ligands, especially those derived from triamines and pyridine-2-aldehyde (or 2-acetylpyridine). The crystal packing of complex **2** is interesting as it forms 1D supramolecular chain through the hydrogen bonding interaction. Both the complexes are moderately active towards the oxidation of *o*-aminophenol, and their relative catalytic efficiency mainly arises from the steric contribution from the ligands, and the electrochemical responses of the metal center. From the experimental data, a nice correlation, wherein the lower the $E_{1/2}$ value the higher the catalytic activity, can be established between $E_{1/2}$ and V_{max} of the complexes. The deuterium kinetic isotope effect in the catalytic oxidative coupling of two moles of OAPH by O_2 as shown by the 1.6 times rate retardation in the deuterated solvent unambiguously suggests hydrogen atom transfer in the rate-determining step from the substrate hydroxy group to the metal-bound superoxo species.

Acknowledgements

A. P. is grateful to the University Grants Commission, India, for the financial support of this research (Sanction no. PSW-173/11-12). Jadavpur University and Indian Association for the Cultivation of Science, India, are also gratefully acknowledged for the instrumentation facilities.

References

- 1 E. Tsuchida and K. Oyaizu, *Coord. Chem. Rev.*, 2003, **237**, 213–228.
- 2 L. Canali and D. C. Sherrington, *Chem. Soc. Rev.*, 1999, **28**, 85–93.
- 3 J. Tisato, F. Refosco and F. Bandoli, *Coord. Chem. Rev.*, 1994, **135**, 325–397.
- 4 R. J. Ferm and J. L. Riebsomer, *Chem. Rev.*, 1954, **54**, 593–613.
- 5 R. J. Ferm, J. L. Riebsomer, E. L. Martin and G. H. Daub, *J. Org. Chem.*, 1953, **18**, 643–648.
- 6 M. Boča, D. Valigura and W. Linert, *Tetrahedron*, 2000, **56**, 441–446.
- 7 S. Deoghoria, S. Sain, M. Soler, W. T. Wong, G. Christou, S. K. Bera and S. K. Chandra, *Polyhedron*, 2003, **22**, 257–262.
- 8 M. Boča, P. Baran, R. Boca, G. Kickelbick, F. Renz and W. Linert, *Inorg. Chem. Commun.*, 1999, **2**, 188–190.
- 9 M. Boča, P. Baran, R. Boca, M. Fuess, G. Kickelbick, W. Linert, F. Renz and I. Svoboda, *Inorg. Chem.*, 2000, **39**, 3205–3212.
- 10 N. Bréfuel, C. Lepetit, S. Shova, F. Dahan and J.-P. Tuchagues, *Inorg. Chem.*, 2005, **44**, 8916–8928.
- 11 A. Panja and P. Guionneau, *Dalton Trans.*, 2013, 5068–5075.
- 12 A. Panja, M. Shyamal, A. Saha and T. K. Mandal, *Dalton Trans.*, 2014, 5443–5452.
- 13 A. Panja, *Polyhedron*, 2014, **80**, 81–89.
- 14 A. Panja, *Dalton Trans.*, 2014, 7760–7770.
- 15 A. Panja, *Polyhedron*, 2014, **79**, 258–268.

- 16 E. I. Solomon, T. C. Brunold, M. I. Davis, J. N. Kemsley, S. K. Lee, N. Lehnert, F. Neese, A. J. Skulan, Y. S. Yang and J. Zhou, *Chem. Rev.*, 2000, **100**, 235–349.
- 17 E. I. Solomon, R. Sarangi, J. S. Woertink, A. J. Augustine, J. Yoon and S. Ghosh, *Acc. Chem. Res.*, 2007, **40**, 581–591.
- 18 E. G. Kovaleva and J. D. Lipscomb, *Nat. Chem. Biol.*, 2008, **4**, 186–193.
- 19 C. E. Barry, P. G. Nayar and T. P. Begley, *Biochemistry*, 1989, **28**, 6323–6333.
- 20 A. W. Smith, A. Camara-Artigas, M. Wang, J. P. Allen and W. A. Francisco, *Biochemistry*, 2006, **45**, 4378–4387.
- 21 C. E. Barry, P. G. Nayar and T. P. Begley, *J. Am. Chem. Soc.*, 1988, **110**, 3333–3342.
- 22 E. Frei, *Cancer Chemother. Rep., Part 1*, 1974, **58**, 49–54.
- 23 U. Hollstein, *Chem. Rev.*, 1974, **74**, 625–652.
- 24 L. I. Simándi, T. M. Simándi, Z. May and G. Bensenyei, *Coord. Chem. Rev.*, 2003, **245**, 85–93.
- 25 M. Hassanein, M. Abdo, S. Gerges and S. El-Khalafy, *J. Mol. Catal. A: Chem.*, 2008, **287**, 53–56.
- 26 R. Bakshi, R. Kumar and P. Mathur, *Catal. Commun.*, 2012, **17**, 140–145.
- 27 C. Mukherjee, T. Weyhermuller, E. Bothe, E. Rentschler and P. Chaudhuri, *Inorg. Chem.*, 2007, **46**, 9895–9905.
- 28 T. M. Simándi, L. I. Simándi, M. Győr, A. Rockenbauer and Á. Gömör, *Dalton Trans.*, 2004, 1056–1060.
- 29 T. Horváth, J. Kaizer and G. Speier, *J. Mol. Catal. A: Chem.*, 2004, **215**, 9–15.
- 30 J. Kaizer, G. Baráth, R. Csonka, G. Speier, L. Korecz, A. Rockenbauer and L. Párkányi, *J. Inorg. Biochem.*, 2008, **102**, 773–780.
- 31 C. Mukherjee, T. Weyhermüller, E. Bothe and P. Chaudhuri, *C. R. Chim.*, 2007, **10**, 313–325.
- 32 G. M. Sheldrick, *SAINTE, Version 6.02, SADABS, Version 2.03*, Bruker AXS Inc., Madison, Wisconsin, 2002.
- 33 G. M. Sheldrick, *SHELXL97*, Program for Crystal Structure Refinement, University of Göttingen, Göttingen, Germany, 1997.
- 34 L. J. Farrugia, *J. Appl. Crystallogr.*, 1999, **32**, 837–838.
- 35 Y.-M. Lee, E.-S. Kim, H.-J. Kim, H. J. Choi, Y.-I. Kim, S. K. Kang and S.-N. Choi, *Dalton Trans.*, 2009, 126–133.
- 36 S. E. Ghachtouli, A. Mohamadou and J.-P. Barbier, *Inorg. Chim. Acta*, 2005, **358**, 3873–3880.
- 37 S. I. M. Paris, Ü. A. Laskay, S. Liang, O. Pavlyuk, S. Tschirschwitz, P. Lönnecke, M. C. McMills, G. P. Jackson, J. L. Petersen, E. Hey-Hawkins and M. P. Jensen, *Inorg. Chim. Acta*, 2010, **363**, 3390–3398.
- 38 C. Hureau, S. Groni, R. Guillot, G. Blondin, C. Duboc and E. Anxolabéhère-Mallart, *Inorg. Chem.*, 2008, **47**, 9238–9247.
- 39 S. Groni, C. Hureau, R. Guillot, G. Blondin, G. Blainand and E. Anxolabéhère-Mallart, *Inorg. Chem.*, 2008, **47**, 11783–11797.
- 40 C. Hureau, G. Blondin, M.-F. Charlot, C. Philouze, M. Nierlich, M. Césarío and E. Anxolabéhère-Mallart, *Inorg. Chem.*, 2005, **44**, 3669–3683.